Published in final edited form as:
J Magn Reson Imaging. 2008 February ; 27(2): 299–310. doi:10.1002/jmri.21263.

Stem Cell Therapy: MRI Guidance and Monitoring

Dara L. Kraitchman, VMD, PhD[1,*], **Wesley D. Gilson, PhD**[2], and **Christine H. Lorenz, PhD**[2]

[1]Johns Hopkins University, School of Medicine, Russell H. Morgan Department of Radiology and Radiological Science, Baltimore, Maryland. [2]Siemens Corporate Research, Inc., Department of Imaging and Visualization, Baltimore, Maryland.

Abstract

With the recent advances in magnetic resonance (MR) labeling of cellular therapeutics, it is natural that interventional MRI techniques for targeting would be developed. This review provides an overview of the current methods of stem cell labeling and the challenges that are created with respect to interventional MRI administration. In particular, stem cell therapies will require specialized, MR-compatible devices as well as integration of graphical user interfaces with pulse sequences designed for interactive, real-time delivery in many organs. Specific applications that are being developed will be reviewed as well as strategies for future translation to the clinical realm.

Keywords

interventional MRI; stem cells; cardiac

Because of the limited regenerative capacity of many organs, the exogenous administration of cells offers the promise of repair or renewal after an ischemic or destructive insult. Another mechanism of cellular repair may be the release of cytokines and factors that recruit native cells to the site of injury more robustly, leading to enhanced or accelerated repair or decreased remodeling and/or native cell destruction. While the fate of stem cell therapeutics in animal models may be determined using postmortem histology, patient trials will require less invasive methods. The recent ability to label stem cells with conventional MR-visible contrast agents can provide a method to initially localize the stem cell. Furthermore, serial imaging provides the means to track stem cell persistence and migration over time. Advances in interventional MRI over the last decade enable faster image acquisition and reconstruction for more advanced applications. In addition, both custom and conventional devices for the delivery of therapeutics have been tested for targeting of stem cells by MRI. These advances in interventional hardware and software for the MR-guidance of labeled stem cell therapeutics are examined in this review.

AGENTS FOR MR LABELING

A wide variety of MR contrast agents have been used with varying success for labeling stem cells (1–14). Several good review articles are available that provide detailed descriptions of potential contrast agents for molecular imaging (15) and stem cell labeling (16–19). In general, iron oxide-based contrast agents are favored over conventional paramagnetic agents

[*]Address reprint requests to: D.L.K., VMD, PhD, 601 N. Caroline St., JHOC 4231, Baltimore, MD 21287. dkraitc1@jhu.edu.

because a small number of these nanoparticles can create strong disruptions in the local magnetic field and subsequently produce detectable susceptibility-based image artifacts. Moreover, if the iron oxide label is lost from the cell, it can be eliminated through normal iron recycling mechanisms. However, new formulations of paramagnetic agents have recently been developed with enhanced relaxivity that may partially overcome issues of sensitivity to the label (8–10,20,21). The advantage of paramagnetic contrast agents over iron oxides is that they can be used to shorten T_1 and, thereby, create a hyperintense signal rather than a hypointense signal. Nonetheless, the development of paramagnetic agents for stem cell labeling are also hindered by concerns about gadolinium toxicity should dechelation occur either due to breakdown within endosomes or after stem cell death. A possible alternative is to create positive contrast with iron oxide by imaging the off-resonance effects (Fig. 1) (22–25).

Most stem cell-labeling techniques to date have used direct labeling techniques. Because nearly all stem cells are nonphagocytic, the efficiency of cellular uptake of the contrast agent is enhanced by coating the contrast agent with a transfection agent, such as protamine sulfate or poly-L-lysine (2,4). The cells are incubated with the contrast agent-transfection agent complex for ≈24 hours ex vivo prior to implantation. The use of transfection agents not only leads to more efficient cellular labeling, but also enhanced viability of the cells (26,27). A more recent method to shuttle contrast agents into the cell without the requirement of long incubation times is magnetoelectroporation (MEP) (28). MEP uses small, pulsed voltages to perturb the cell membrane, promoting endocytosis of the contrast agent. The primary advantage of direct labeling techniques is their simplicity. The primary disadvantage of direct labeling techniques is that the label may become dissociated from the cell with cell death or cell fusion. Thus, the inference that the detection of signal intensities associated with the label implies the presence of stem cells may be incorrect (16). However, in practice the contrast agent typically cannot be taken up by cells other than phagocytic cells. Moreover, it is unlikely that the appearance by MRI of the label in phagocytic cells will either be sufficient for detection or will appear similar to ex vivo labeled stem cells (3). Direct labeling techniques may also be complicated by label dilution with cell division. Thus, if stem cell therapies are successful at regenerating tissue, then it can be anticipated that the label dilution with cell replication may impair the ability to detect the stem cell.

Recently, fluorine nanoparticles have been introduced for direct cell labeling (29). These particles can be readily phagocytized by stem and progenitor cells (30). While ^{19}F MRI and MR spectroscopy have the advantage that there is no native fluorine signal in the body, they do require specialized coils and hardware for broadband spectroscopy. At present, stem cells labeled with ^{19}F have not yet been demonstrated in vivo.

Stem Cell Tracking

The first in vivo studies demonstrating the ability to label fetal tissue or stem and progenitor cells with iron nanoparticles and track them over time using MRI were performed in the brain (31–37). In one study, iron oxide-labeled oligodendrocyte progenitor cells were injected bilaterally into the ventricles of the demyelinated rat brain. Migration to the surrounding parenchyma was observed using a 4.7T MR scanner (35). In another study, migration of iron oxide-labeled embryonic stem cells from the nonischemic hemisphere to the ischemic hemisphere in a rat model of stroke in as little as 3 weeks was also demonstrated using a 7T MR scanner (36).

Cardiac MRI tracking of stem cells labeled with iron oxide nanoparticles that were blindly delivered to the heart using conventional x-ray fluoroscopic delivery techniques quickly followed the initial neurological studies (38,39). MRI tracking in the heart was performed at clinical field strengths in large animals with acute myocardial infarction, demonstrating

promise for future clinical cardiovascular applications (Fig. 2) (38,39). In another study, electromechanical mapping systems in combination with x-ray fluoroscopy was used to guide iron-labeled stem cells to specific regions of the myocardium in a swine acute myocardial infarction model (40). While many studies have been performed demonstrating tracking of labeled stem cells in rodents, one study of note involved iron oxide-labeled mesenchymal stem cells (MSCs) delivered into the renal artery of healthy rats and into the portal system of a rat model of liver necrosis and inflammation (41). This study found that a significant number of mesenchymal stem cells were trapped in the renal cortex and sinusoids of the liver. This finding was determined to be due to the large size of the MSCs. Recently, iron oxide-labeled MSCs have been seeded into tissue scaffolds (42) and tracked in vitro over 1 month (43). These engineered tissues with labeled stem cells could ultimately play a role in tissue grafts or whole-organ transplants.

Sex-mismatched organ transplantation has supported the idea of stem cell “homing” to sites of tissue injury (44,45). Recently, this concept was tested using MR-labeled stem cells. A rat model of nephropathy has shown homing of iron oxide-labeled MSCs injected intravenously to the kidney using ex vivo MRI but failed to visualize the cells in vivo (46). A canine study that used intravenously administered MSCs dual-labeled with a radiotracer and iron oxide nanoparticles demonstrated homing of the cells to the heart after myocardial infarction using radionuclide imaging but not using MRI (47). These studies point to the detection threshold of $\approx 10^5$ iron oxide-labeled stem cells for MRI in practical applications in the thorax and abdomen (17,39). This detection threshold is dependent on the spatial and temporal resolution as well as the magnetic field strength. In theory, single-cell detection is possible under ideal conditions, especially in organs where motion can be minimized, such as the brain (48–50). It has further been suggested that the administration of paramagnetic contrast agents prior to imaging can improve the detection of hypointensities from iron oxide-labeled stem cells (51).

Clinical translation of iron oxide labeling of cellular therapies has now been performed. Adoption of iron oxide labeling by regulatory agencies for use in patients was aided by the common use of magnetic bead cell selection in transplant patients, which has been shown to create weak hypointensities on MRI (52,53). In the first study, dendritic cells were colabeled with a clinical formulation of a radiotracer and an iron oxide (Endorem, Guerbet, France) (54). This study demonstrated the power of MRI tracking by revealing that cellular injections into lymph nodes under ultrasound guidance failed in 50% of the patients (54). Furthermore, this study demonstrated the advantage of the higher spatial resolution and soft-tissue detail of MRI compared to SPECT imaging. In a second study, MRI was used to track iron oxide-labeled autologous neural stem cells transplanted in the brain of two patients (55). While these early applications of MR-labeled cellular therapies are promising, the ability to combine cell tracking with MR-guided cell delivery provides the promise of enhanced targeting of stem cell therapeutics.

TARGETING CELL THERAPEUTICS WITH INTERVENTIONAL MRI

Stem Cell Delivery Devices

The most efficacious method of therapeutic stem cell delivery remains unknown. Intravenous delivery is advantageous for ease of delivery, but the concentration of cells that reach the target site can be quite limited. Intraarterial delivery has been used extensively, particularly for treating myocardial infarction, in order to deliver therapeutic cells to the target vessel region. Targeted organ injections are the most direct method of stem cell delivery and could benefit from MRI guidance.

In general, interventional MRI-guided procedures have taken their lead from x-ray fluoroscopic delivery approaches where a variety of devices have been approved specifically for the administration of gene, protein, and stem cell therapeutics (56). At present, modifications to these catheters for MR-compatibility or custom-made devices have been developed primarily for cardiovascular transmyocardial applications in academic centers (38,57–59). The present lack of commercial interest in MR-compatible device development represents a major obstacle to interventional MRI translation into the clinics.

Transmyocardial delivery devices that have been developed for interventional MRI applications have fallen into two classes of devices: passive and active catheters (60–62). The simplest passive catheter system was comprised of an introducer sheath, a stainless steel needle, and a conventional polyethylene catheter, and the catheter was guided to the endocardial surface based on hypointensities created by the needle (63). Another passive catheter implementation involved adding three gadolinium-oxide markers to a prototype, steerable injection catheter with a nitinol needle (Bio-heart, Sunrise, FL) (59). Left ventricular catheterization was performed with this catheter using both x-ray and MR-guidance in a hybrid x-ray/MR fluoroscopy suite. A more elegant combination active/passive system was developed using an FDA-approved active MR loopless antennae (Intercept, Surgi-Vision, Columbia, MD) and a custom guide catheter (AGA Medical, Plymouth, MN) to catheterize the left ventricle. The active guidewire was then replaced with a FDA-approved conventional injection needle (Stiletto, Boston Scientific, Natick, MA) composed of nitinol, which creates a signal void in the images during targeting (64). While the hypointensities created by passive devices may be acceptable in these proof-of-principle demonstrations using injections of paramagnetic contrast agents, the ability to distinguish the needle tip from hypointensities created by iron-labeled cells may be problematic.

Several active catheter systems have been developed. One approach involved modifying a steerable guide catheter with an injection needle (Stiletto, Boston Scientific) to contain active receive-only coils (57). Hardware modifications allowed the combination of this active injection catheter with conventional surface coils to enable imaging the full thoracic anatomy rather than just imaging the localized anatomy around the active catheter. Further enhancements to this device included additional receiver coils to allow both the injection needle and guide catheter to be easily localized (Fig. 3) (58,65). Another active catheter design included an active needle consisting of a loopless antenna that was also combined with conventional surface coils (66). Tuning and matching circuitry were placed at the distal end of the device to minimize device size. Enhanced steerability was created by the use of a pull-wire mechanism. One advantage of this design was that a long length of the device was visible during guidance. The disadvantage of this design, as in some x-ray injection devices, is that the needle lumen could not accommodate a guidewire.

While active devices produce a high signal intensity for tracking, there are always concerns about heating of the device (67). However, preliminary studies of specific absorption rates using a custom, active loopless antennae injection device have only shown excessive heating associated with extension of the needle beyond the catheter (66). With insulation of the needle, the heating observed in this active catheter system could be significantly reduced. A possible solution to these heating concerns has been demonstrated by Weiss et al (68) using an optically detunable resonant marker on the catheter tip. However, steerable catheters for stem cell injections will require several markers to adequately track the catheter length and tip.

Imaging Sequences

For rapid real-time imaging, most interventional vascular MR applications have used steady-state free precession (SSFP) techniques (69). SSFP imaging is amenable to real-time

imaging because it yields high signal-to-noise, fast image acquisition rates, high spatial resolution, and high contrast between tissue and blood due to T_2/T_1 weighting (70). SSFP acquisitions have been performed using traditional rectilinear, radial (71), and spiral (72) *k*-space trajectories. In addition, keyhole imaging and view-sharing have been used to enhance temporal resolution during MR fluoroscopy (73–75). While parallel imaging techniques (76,77) offer another means to increase temporal resolution, the reduction in signal-to-noise may impart too severe a penalty for many real-time stem cell applications. Inversion recovery, saturation recovery, and fat saturation prepulses can also be useful for T_1-weighted images of test gadolinium injections prior to stem cell injections during targeting (57). Typically, images are acquired without cardiac or respiratory gating to obtain the highest possible frame rate. More details about imaging sequences for interventional MRI are covered by Elgort and Duerk (78).

For serial interrogation of the efficacy of the stem cell therapy, a variety of conventional MRI examinations can be performed. In the heart, cine MRI for the calculation of measurements of global function as well as tagged or DENSE imaging for the determination of regional myocardial function may be performed (79–83). Also, first-pass contrast-enhanced MRI to determine local myocardial perfusion and delayed contrast-enhanced MRI for the evaluation of infarct size are typically performed (84,85). Serial tracking of the stem cells will depend on the labeling methodology. For iron oxide-labeled cells, T_2*-weighted image sequences, which magnify the blooming artifact from the label, are most commonly used to serially track cells in the brain, kidneys, tumors, liver, and heart (38,39,41,86–92).

Imaging Platforms and Interfaces—The interventional MRI platform requires the coordination of MR-compatible devices, real-time imaging sequences, graphical interfaces, scanner controls, and physiological monitoring into one efficient package for stem cell delivery applications. For example, previously acquired delayed contrast-enhanced MRI for infarct localization can be used to target cellular injections to regions surrounding the infarction while watching physiological monitors for the development of arrhythmias during needle advancement and injections. Additional useful features include: 1) the ability to colorize the active catheter and needle components and overlay them on grayscale anatomical images; 2) the display of road map images with real-time images; 3) interactive scan plane manipulation; and 4) pulse sequence parameter manipulation during real-time scanning (93–95). All three major MR scanner vendors are developing graphical interfaces to accommodate many of these features. A representative screen-shot of an interface is shown in Fig. 4 (96,97). Some advanced features may include the ability to perform automatic image plane updating based on tracking catheter locations, tip tracking, and image field-of-view determination dependent on the speed of catheter motion (98–101). Other useful features that have been incorporated into some packages include physiological monitoring and temperature from optical sensors or using advanced MRI methods (102,103). At present, manipulation of the catheter probes by robotic devices has not yet been used in stem cell applications, but has been used for needle-based procedures in other parts of the body (104).

Role of Interventional MRI in Stem Cell Therapy

The earliest applications of interventional MRI for targeted injections did not inject stem cells, but rather determined the accuracy of stem cell targeting using injections of MR contrast agents with visible dyes for validation in phantoms and postmortem (Fig. 5) (57,59,63–66,105,106). These studies documented the ability to determine the immediate success or failure of injections into the myocardium with failure rates ranging from 0%–19%. However, due to the wash-out of the gadolinium-based agents from the tissue, the MRI enhancement patterns from multiple injections persisted for only 10–20 minutes (Fig. 6) and

could potentially be confounded by hyperintensities due to delayed contrast- enhanced imaging.

A significant advantage of interventional MRI combined with iron oxide labeling of cells is the ability to have immediate feedback concerning the success and localization of the injection. Under x-ray fluoroscopy, confirmation of successful transmyocardial delivery of stem cells is essentially impossible. In fact, injection failure rates of 30%–35% under x-ray guidance have been reported using MRI detection of the injections (38,89). The voluntary suspension of a gene therapy trial delivered transmyocardially with a Stiletto catheter has raised concern about the quantity of injectate that should be delivered. Thus, more recent studies have concentrated on delivery of stem cells without test contrast injections (38,58). With MR delivery, soft-tissue detail is enhanced, the injections can be targeted to specific tissues or pathologies based on conventional MR imaging, and the success of the injections can be ascertained in real-time. This has been demonstrated in the heart after acute myocardial infarction (Fig. 7) (38,58). Furthermore, exposure of the naïve stem cells to ionizing radiation can be avoided. Additionally, the efficacy of the stem cell therapy can often be determined using conventional MR imaging protocols with intrinsic registration to the images used for cellular tracking.

Some of the first clinical cardiovascular trials using unlabeled cells were delivered using an intracoronary route via traditional x-ray interventional techniques (107–119). Despite the suggestion by an experimental study of higher cellular retention and engraftment using a transmyocardial delivery route (120), only a limited number of trials have been performed in patients using this delivery route (121–124). Since cardiovascular MRI can identify viable myocardium (125,126), areas that may be preferred for stem cell engraftment can be specifically targeted using interventional MRI and labeled stem cells (127). Several groups have been actively involved in large animal studies on clinical scanners to develop protocols that will assist this effort (58,65,128,129). An x-ray injection system for gene, protein, and cellular therapeutics has been modified for use as an active injection catheter and used for cellular therapeutic injections in a swine model of acute myocardial infarction (58). Tracking and localization of the injection catheter can be enhanced by color coding the receiver from the injection catheter while sequentially obtaining images in multiple planes. Representative still frames from a screen capture movie of an MRI-guided left ventricular catheterization are shown in Fig. 8. The custom, active injection catheter (66) is guided from a carotid artery approach to the infarcted myocardium in a dog using the Siemens Interactive Front End (IFE) graphical interface and interactive real-time SSFP pulse sequence (Fig. 8). Within the graphical interface, one can vary the gain from the active catheter to make it more or less prominent (Fig. 8e–g). In these studies, SSFP imaging was performed during catheter guidance and transendocardial stem cell injection, typically using a frame rate of ≈3–8 frames/sec with a slice thickness of 8–10 mm (Fig. 9) (58,129). Hypointensities appear in real-time as the iron oxide-labeled stem cells are injected in the myocardium and confirm the success of individual injections (Fig. 9). Documentation of the stem cell injection sites can be performed using cardiac gated and breath-hold images acquired with a high spatial resolution either as a 2D stack of images or a 3D volume (Fig. 7).

Stem Cell Efficacy Determined Using MRI

Beyond anatomical imaging, MRI has the added benefit of being able to examine organ functionality and perfusion. In the simplest case, anatomical imaging can be performed to assess organ mass as a surrogate for stem cell tissue regeneration. The functional effects of the stem cells can be assessed using MRI techniques that measure changes in tissue perfusion, tissue oxygenation, or tissue function. In the central nervous system, functional or diffusion MRI, in concert with anatomical imaging, may be used to complement clinical

tests of neurological function to determine whether stem cell therapy resolves or slows the progression of disease.

The effect of stem cell type and route of delivery has been tested most extensively using MRI in acute ischemic disease and chronic heart failure. Of all the noninvasive imaging modalities, MRI is considered superior for assessing myocardial function and myocardial viability. In particular, the high repeatability and accuracy of MRI allow one to demonstrate a statistically significant treatment effect with a much diminished sample size (130).

Several preclinical studies using labeled and unlabeled stem and progenitor cells have used serial MRI to determine efficacy. In a swine model of reperfused myocardial infarction, Amado et al (90) have shown that infarct size by delayed contrast-enhanced MRI was reduced in animals receiving intramyocardial injections of iron oxide-labeled mesenchymal stem cells, but not in animals that did not receive cells. These results run contrary to classical studies of infarct remodeling where infarct expansion in the first week is followed by infarct remodeling and wall thinning (131). Conversely, in a reperfused swine infarction model, Moelker et al (132) were able to demonstrate reductions in infarct size over 4 weeks in both treated and untreated animals with a slight increased reduction in infarct size in those animals that received intracoronary injections of bone-marrow-derived stem cells, but global left ventricular function was not improved by cellular therapy. A representative example of regional myocardial function based on tagged MRI showing little improvement in function despite mesenchymal stem cell therapy is shown in Fig. 10.

In a rat model of permanent coronary occlusion, Limbourg et al (133) showed that intravenous administration of 7500 bone marrow mononuclear cells resulted in improvements in wall shortening and ejection fraction by MRI as early as 3 days postadministration, but only sporadic cells could be detected at 4 weeks postadministration. Infarct size, however, was not different between sham and treated rats (133). Zeng et al (134) have also shown in a rat model of permanent coronary occlusion with a ≈10% loss of left ventricular mass that high-energy phosphates, as measured by PCr/ATP ratios from 31P MRS, were improved in animals that received allogeneic pMultistem cells (135), a class of bone marrow stem cells whose origin has been the subject of much recent controversy (136). Interestingly, 0.35% of these cells were still detected by histology at 4 weeks postinjection, which suggests a poor retention of stem cells whether given by intracoronary or intravenous delivery (134). In a direct intramyocardial injection study of 500,000 iron oxide-labeled MSCs delivered in four injections to the border zone of a nonreperfused infarcted rat, Stuckey et al (89) showed retention at 16 weeks postinjection and suggested that retention of stem cells was higher in the infarcted myocardium. However, more detailed studies in large animals are expected to further elucidate the best location for stem cell injections (88,137). Overall, these data support radiotracer studies of increased stem cell retention with direct intramyocardial injections (120).

Numerous clinical cardiovascular cellular trials have been performed but the vast majority have relied on echocardiographic assessment of left ventricular function. Of the recent randomized clinical trials using MRI, global left ventricular function and/or viability was assessed after treatment with bone marrow mononuclear treatment by intracoronary injection (111,113–116). While most studies were powered primarily to demonstrate safety and not efficacy, provisional efficacy based on sustained improvements in left ventricular ejection fraction was only shown in one study (113). The transmural extent of infarction also appeared to be critical in determining outcomes in another study (114). The enrollment criteria in many of these trials included patients with moderate disease such that the studies were underpowered to demonstrate an effect of the therapy, even using MRI.

In summary, MRI results from both preclinical animal studies (90,132–134) and clinical trials (109,111–116,138–140) have demonstrated that these therapies are safe, but have failed to reach a consensus as to whether stem cell therapy in cardiovascular disease is efficacious. While these results may appear to be contradictory and inconsistent, many variables, such as stem cell type, therapeutic dose, timing of dose, etc., may be the underlying confounders. Thus, while the vast majority of studies have not used labeled stem cells or interventional MRI delivery, it is anticipated that the addition or combination of these techniques will lead to a better understanding of the cellular therapy, targeting, and assessment of stem cell therapies with the end result of optimized therapeutic protocols.

LIMITATIONS

Several limitations still exist in the translation of preclinical interventional MRI studies with labeled stem cells to the expanding number of clinical trials. While two studies have been performed with direct labeling of cells with iron oxide compounds in patients, the potential for the iron oxide to become uncoupled from the exogenously labeled stem cell can lead to inaccurate tracking results after serial delivery. Another concern with iron oxide-labeled stem cells is the ability to distinguish hypointensities associated with the cells from changes in T_1 and T_2 due to edema, inflammation, and hemorrhage secondary to acute ischemia (141). Kustermann et al (142) have shown that the area of hypointensity on proton density and T_2* images is dissimilar where iron oxide-labeled progenitor cells have been delivered, whereas areas without cells show no such variation in hypointensity. Whether this simple method to distinguish cells from other causes of hypointensities will succeed in clinical trials remains to be tested. Thus, direct labeling is simple, has been developed with clinical grade compounds, and is amenable to clinical trials.

Another area of concern is the lack of commercial testing and development of MR-compatible devices for interventional MRI. Without such industry support, the future of interventional MRI will remain tenuous. Despite the numerous advantages of MRI delivery, concerns about the ability to monitor patients in the MRI environment, the potential for active device heating leading to either loss of stem cell viability or patient burns, and the frequent placement of MRI facilities away from traditional interventional and surgical suites have also limited the rapid expansion of these techniques. Thus, it is likely that in the near future labeled stem cell therapies will move into clinical trials with interventional MRI delivery of labeled stem cells following at a less rapid pace.

Acknowledgments

The authors thank Elliot McVeigh, PhD, and Michael Guttman, MS, for assistance in the MR-guided stem cell experiments shown in Figures 4, 8, and 9 and for many helpful discussions on the interface design. The authors also thank Sven Zuehlsdorff, PhD, and Peter Speier, PhD, for the interactive real-time pulse sequence.

Contract grant sponsor: National Institutes of Health (NIH); Contract grant numbers: NIH/NLHBI-R01-HL073223, NIH/NHLBI-R01-HL056882, NIH/NHLBI-R01-HL072704, and NIH/NIBIB-R01-EB007825 (to D.L.K.).

REFERENCES

1. Lewin M, Carlesso N, Tung CH, et al. Tat peptide-derivatized magnetic nanoparticles allow in vivo tracking and recovery of progenitor cells. Nat Biotechnol. 2000; 18:410–414. [PubMed: 10748521]
2. Frank JA, Zywicke H, Jordan EK, et al. Magnetic intracellular labeling of mammalian cells by combining (FDA-approved) super-paramagnetic iron oxide MR contrast agents and commonly used transfection agents. Acad Radiol. 2002; 9 Suppl 2:S484–S487. [PubMed: 12188316]
3. Hinds KA, Hill JM, Shapiro EM, et al. Highly efficient endosomal labeling of progenitor and stem cells with large magnetic particles allows magnetic resonance imaging of single cells. Blood. 2003; 102:867–872. [PubMed: 12676779]

4. Frank JA, Miller BR, Arbab AS, et al. Clinically applicable labeling of mammalian and stem cells by combining superparamagnetic iron oxides and transfection agents. Radiology. 2003; 228:480–487. [PubMed: 12819345]
5. Frank JA, Anderson SA, Kalsih H, et al. Methods for magnetically labeling stem and other cells for detection by in vivo magnetic resonance imaging. Cytotherapy. 2004; 6:621–625. [PubMed: 15773025]
6. Arbab AS, Yocum GT, Kalish H, et al. Efficient magnetic cell labeling with protamine sulfate complexed to ferumoxides for cellular MRI. Blood. 2004; 104:1217–1223. [PubMed: 15100158]
7. Aime S, Barge A, Cabella C, Crich SG, Gianolio E. Targeting cells with MR imaging probes based on paramagnetic Gd(III) chelates. Curr Pharm Biotechnol. 2004; 5:509–518. [PubMed: 15579040]
8. Vuu K, Xie J, McDonald MA, et al. Gadolinium-rhodamine nanoparticles for cell labeling and tracking via magnetic resonance and optical imaging. Bioconjug Chem. 2005; 16:995–999. [PubMed: 16029042]
9. Giesel FL, Stroick M, Griebe M, et al. Gadofluorine m uptake in stem cells as a new magnetic resonance imaging tracking method: an in vitro and in vivo study. Invest Radiol. 2006; 41:868–873. [PubMed: 17099425]
10. Anderson SA, Lee KK, Frank JA. Gadolinium-fullerenol as a paramagnetic contrast agent for cellular imaging. Invest Radiol. 2006; 41:332–338. [PubMed: 16481917]
11. Ben-Hur T, van Heeswijk RB, Einstein O, et al. Serial in vivo MR tracking of magnetically labeled neural spheres transplanted in chronic EAE mice. Magn Reson Med. 2007; 57:164–171. [PubMed: 17191231]
12. Brekke C, Morgan SC, Lowe AS, et al. The in vitro effects of a bimodal contrast agent on cellular functions and relaxometry. NMR Biomed. 2007; 20:77–89. [PubMed: 16952123]
13. Lu CW, Hung Y, Hsiao JK, et al. Bifunctional magnetic silica nanoparticles for highly efficient human stem cell labeling. Nano Lett. 2007; 7:149–154. [PubMed: 17212455]
14. Shyu WC, Chen CP, Lin SZ, Lee YJ, Li H. Efficient tracking of non-iron-labeled mesenchymal stem cells with serial MRI in chronic stroke rats. Stroke. 2007; 38:367–374. [PubMed: 17194887]
15. Wickline SA, Neubauer AM, Winter PM, Caruthers SD, Lanza GM. Molecular imaging and therapy of atherosclerosis with targeted nanoparticles. J Magn Reson Imaging. 2007; 25:667–680. [PubMed: 17347992]
16. Bulte JW, Kraitchman DL. Iron oxide MR contrast agents for molecular and cellular imaging. NMR Biomed. 2004; 17:484–499. [PubMed: 15526347]
17. Bulte JW, Kraitchman DL. Monitoring cell therapy using iron oxide MR contrast agents. Curr Pharm Biotechnol. 2004; 5:567–584. [PubMed: 15579045]
18. Zhou R, Acton PD, Ferrari VA. Imaging stem cells implanted in infarcted myocardium. J Am Coll Cardiol. 2006; 48:2094–2106. [PubMed: 17112999]
19. Bengel FM, Schachinger V, Dimmeler S. Cell-based therapies and imaging in cardiology. Eur J Nucl Med Mol Imaging. 2005; 32 Suppl 2:S404–S416. [PubMed: 16205898]
20. Rudelius M, Daldrup-Link HE, Heinzmann U, et al. Highly efficient paramagnetic labelling of embryonic and neuronal stem cells. Eur J Nucl Med Mol Imaging. 2003; 30:1038–1044. [PubMed: 12567250]
21. Crich SG, Biancone L, Cantaluppi V, et al. Improved route for the visualization of stem cells labeled with a Gd-/Eu-chelate as dual (MRI and fluorescence) agent. Magn Reson Med. 2004; 51:938–944. [PubMed: 15122675]
22. Mani V, Briley-Saebo KC, Itskovich VV, Samber DD, Fayad ZA. Gradient echo acquisition for superparamagnetic particles with positive contrast (GRASP): sequence characterization in membrane and glass superparamagnetic iron oxide phantoms at 1.5T and 3T. Magn Reson Med. 2006; 55:126–135. [PubMed: 16342148]
23. Coristine, AJ.; Foster, P.; Deoni, SC.; Heyn, C.; Rutt, BK. Proc ISMRM. Kyoto, Japan: 2004. Positive contrast labelling of SPIO loaded cells in cell samples and spinal cord injury; p. 163
24. Cunningham CH, Arai T, Yang PC, McConnell MV, Pauly JM, Conolly SM. Positive contrast magnetic resonance imaging of cells labeled with magnetic nanoparticles. Magn Reson Med. 2005; 53:999–1005. [PubMed: 15844142]

25. Stuber M, Gilson WD, Schar M, et al. Positive contrast visualization of iron oxide-labeled stem cells using inversion recovery with on-resonant water suppression (IRON). Magn Reson Med. 2007; 58:1072–1077. [PubMed: 17969120]
26. van den Bos EJ, Wagner A, Mahrholdt H, et al. Improved efficacy of stem cell labeling for magnetic resonance imaging studies by the use of cationic liposomes. Cell Transplant. 2003; 12:743–756. [PubMed: 14653621]
27. Arbab AS, Bashaw LA, Miller BR, Jordan EK, Bulte JW, Frank JA. Intracytoplasmic tagging of cells with ferumoxides and transfection agent for cellular magnetic resonance imaging after cell transplantation: methods and techniques. Transplantation. 2003; 76:1123–1130. [PubMed: 14557764]
28. Walczak P, Kedziorek DA, Gilad AA, Lin S, Bulte JW. Instant MR labeling of stem cells using magnetoelectroporation. Magn Reson Med. 2005; 54:769–774. [PubMed: 16161115]
29. Ahrens ET, Flores R, Xu H, Morel PA. In vivo imaging platform for tracking immunotherapeutic cells. Nat Biotechnol. 2005; 23:983–987. [PubMed: 16041364]
30. Partlow KC, Chen J, Brant JA, et al. 19F magnetic resonance imaging for stem/progenitor cell tracking with multiple unique perfluorocarbon nanobeacons. FASEB J. 2007; 21:1647–1654. [PubMed: 17284484]
31. Norman AB, Thomas SR, Pratt RG, Lu SY, Norgren RB. Magnetic resonance imaging of neural transplants in rat brain using a superparamagnetic contrast agent. Brain Res. 1992; 594:279–283. [PubMed: 1450953]
32. Hawrylak N, Ghosh P, Broadus J, Schlueter C, Greenough WT, Lauterbur PC. Nuclear magnetic resonance (NMR) imaging of iron oxide-labeled neural transplants. Exp Neurol. 1993; 121:181–192. [PubMed: 8339769]
33. Bulte JW, Zhang S, van Gelderen P, et al. Neurotransplantation of magnetically labeled oligodendrocyte progenitors: magnetic resonance tracking of cell migration and myelination. Proc Natl Acad Sci U S A. 1999; 96:15256–15261. [PubMed: 10611372]
34. Franklin RJ, Blaschuk KL, Bearchell MC, et al. Magnetic resonance imaging of transplanted oligodendrocyte precursors in the rat brain. Neuroreport. 1999; 10:3961–3965. [PubMed: 10716241]
35. Bulte JW, Douglas T, Witwer B, et al. Magnetodendrimers allow endosomal magnetic labeling and in vivo tracking of stem cells. Nat Biotechnol. 2001; 19:1141–1147. [PubMed: 11731783]
36. Hoehn M, Kustermann E, Blunk J, et al. Monitoring of implanted stem cell migration in vivo: a highly resolve in vivo magnetic resonance imaging investigation of experimental stroke in rat. Proc Natl Acad Sci U S A. 2002; 25:16267–16772. [PubMed: 12444255]
37. Zhang ZG, Jiang Q, Zhang R, et al. Magnetic resonance imaging and neurosphere therapy of stroke in rat. Ann Neurol. 2003; 53:259–263. [PubMed: 12557295]
38. Kraitchman DL, Heldman AW, Atalar E, et al. In vivo magnetic resonance imaging of mesenchymal stem cells in myocardial infarction. Circulation. 2003; 107:2290–2293. [PubMed: 12732608]
39. Hill JM, Dick AJ, Raman VK, et al. Serial cardiac magnetic resonance imaging of injected mesenchymal stem cells. Circulation. 2003; 108:1009–1014. [PubMed: 12912822]
40. Garot J, Unterseeh T, Teiger E, et al. Magnetic resonance imaging of targeted catheter-based implantation of myogenic precursor cells into infarcted left ventricular myocardium. J Am Coll Cardiol. 2003; 41:1841–1846. [PubMed: 12767674]
41. Bos C, Delmas Y, Desmouliere A, et al. In vivo MR imaging of intravascularly injected magnetically labeled mesenchymal stem cells in rat kidney and liver. Radiology. 2004; 233:781–789. [PubMed: 15486216]
42. Ko IK, Song HT, Cho EJ, Lee ES, Huh YM, Suh JS. In vivo MR imaging of tissue-engineered human mesenchymal stem cells transplanted to mouse: a preliminary study. Ann Biomed Eng. 2007; 35:101–108. [PubMed: 17111211]
43. Terrovitis JV, Bulte JW, Sarvananthan S, et al. Magnetic resonance imaging of ferumoxide-labeled mesenchymal stem cells seeded on collagen scaffolds-relevance to tissue engineering. Tissue Eng. 2006; 12:2765–2775. [PubMed: 17518646]

44. Laflamme MA, Myerson D, Saffitz JE, Murry CE. Evidence for cardiomyocyte repopulation by extracardiac progenitors in transplanted human hearts. Circ Res. 2002; 90:634–640. [PubMed: 11934829]
45. Deb A, Wang S, Skelding KA, Miller D, Simper D, Caplice NM. Bone marrow-derived cardiomyocytes are present in adult human heart A study of gender-mismatched bone marrow transplantation patients. Circulation. 2003; 107:1247–1249. [PubMed: 12628942]
46. Hauger O, Frost EE, van Heeswijk R, et al. MR evaluation of the glomerular homing of magnetically labeled mesenchymal stem cells in a rat model of nephropathy. Radiology. 2006; 238:200–210. [PubMed: 16373768]
47. Kraitchman DL, Tatsumi M, Gilson WD, et al. Dynamic imaging of allogeneic mesenchymal stem cells trafficking to myocardial infarction. Circulation. 2005; 112:1451–1461. [PubMed: 16129797]
48. Foster-Gareau P, Heyn C, Alejski A, Rutt BK. Imaging single mammalian cells with a 1.5 T clinical MRI scanner. Magn Reson Med. 2003; 49:968–971. [PubMed: 12704781]
49. Zhang Z, van den Bos EJ, Wielopolski PA, de Jong-Popijus M, Duncker DJ, Krestin GP. High-resolution magnetic resonance imaging of iron-labeled myoblasts using a standard 1.5-T clinical scanner. Magma. 2004; 17:201–209. [PubMed: 15517471]
50. Shapiro EM, Sharer K, Skrtic S, Koretsky AP. In vivo detection of single cells by MRI. Magn Reson Med. 2006; 55:242–249. [PubMed: 16416426]
51. Baklanov DV, Demuinck ED, Thompson CA, Pearlman JD. Novel double contrast MRI technique for intramyocardial detection of percutaneously transplanted autologous cells. Magn Reson Med. 2004; 52:1438–1442. [PubMed: 15562483]
52. Ruhparwar A, Ghodsizad A, Niehaus M, et al. Clinically applicable 7-Tesla magnetic resonance visualization of transplanted human adult stem cells labeled with CliniMACS nanoparticles. Thorac Cardiovasc Surg. 2006; 54:447–451. [PubMed: 17089310]
53. Weber A, Pedrosa I, Kawamoto A, et al. Magnetic resonance mapping of transplanted endothelial progenitor cells for therapeutic neovascularization in ischemic heart disease. Eur J Cardiothorac Surg. 2004; 26:137–143. [PubMed: 15200992]
54. de Vries IJ, Lesterhuis WJ, Barentsz JO, et al. Magnetic resonance tracking of dendritic cells in melanoma patients for monitoring of cellular therapy. Nat Biotechnol. 2005; 23:1407–1413. [PubMed: 16258544]
55. Zhu J, Zhou L, XingWu F. Tracking neural stem cells in patients with brain trauma. N Engl J Med. 2006; 355:2376–2378. [PubMed: 17135597]
56. Sherman W, Martens TP, Viles-Gonzalez JF, Siminiak T. Catheter-based delivery of cells to the heart. Nat Clin Pract Cardiovasc Med. 2006; (3 Suppl 1):S57–S64. [PubMed: 16501633]
57. Lederman RJ, Guttman MA, Peters DC, et al. Catheter-based endomyocardial injection with real-time magnetic resonance imaging. Circulation. 2002; 105:1282–1284. [PubMed: 11901036]
58. Dick AJ, Guttman MA, Raman VK, et al. Magnetic resonance fluoroscopy allows targeted delivery of mesenchymal stem cells to infarct borders in Swine. Circulation. 2003; 108:2899–2904. [PubMed: 14656911]
59. Saeed M, Lee R, Martin A, et al. Transendocardial delivery of extracellular myocardial markers by using combination x-ray/MR fluoroscopic guidance: feasibility study in dogs. Radiology. 2004; 231:689–696. [PubMed: 15163809]
60. McKinnon GC, Debatin JF, Leung DA, Wildermuth S, Holtz DJ, von Schulthess GK. Towards active guidewire visualization in interventional magnetic resonance imaging. Magma. 1996; 4:13–18. [PubMed: 8773997]
61. Dumoulin CL, Souza SP, Darrow RD. Real-time position monitoring of invasive devices using magnetic resonance. Magn Reson Med. 1993; 29:411–415. [PubMed: 8450752]
62. Zhang S, Rafie S, Chen Y, et al. In vivo cardiovascular catheterization under real-time MRI guidance. J Magn Reson Imaging. 2006; 24:914–917. [PubMed: 16941633]
63. Krombach GA, Pfeffer JG, Kinzel S, Katoh M, Gunther RW, Buecker A. MR-guided percutaneous intramyocardial injection with an MR-compatible catheter: feasibility and changes in T1 values after injection of extracellular contrast medium in pigs. Radiology. 2005; 235:487–494. [PubMed: 15858090]

64. Rickers C, Gallegos R, Seethamraju RT, et al. Applications of magnetic resonance imaging for cardiac stem cell therapy. J Interv Cardiol. 2004; 17:37–46. [PubMed: 15009770]
65. Saeed M, Martin AJ, Lee RJ, et al. MR guidance of targeted injections into border and core of scarred myocardium in pigs. Radiology. 2006; 240:419–426. [PubMed: 16801371]
66. Karmarkar PV, Kraitchman DL, Izbudak I, et al. MR-trackable intramyocardial injection catheter. Mag Reson Med. 2004; 51:1163–1172.
67. Yeung CJ, Atalar E. RF transmit power limit for the barewire loopless catheter antenna. J Magn Reson Imaging. 2000; 12:86–91. [PubMed: 10931568]
68. Weiss S, Kuehne T, Brinkert F, et al. In vivo safe catheter visualization and slice tracking using an optically detunable resonant marker. Magn Reson Med. 2004; 52:860–868. [PubMed: 15389956]
69. Busse RF, Riederer SJ. Steady-state preparation for spoiled gradient echo imaging. Magn Reson Med. 2001; 45:653–661. [PubMed: 11283994]
70. Duerk JL, Lewin JS, Wendt M, Petersilge C. Remember true FISP? A high SNR, near 1-second imaging method for T2-like contrast in interventional MRI at 2 T. J Magn Reson Imaging. 1998; 8:203–208. [PubMed: 9500281]
71. Peters DC, Lederman RJ, Dick AJ, et al. Undersampled projection reconstruction for active catheter imaging with adaptable temporal resolution and catheter-only views. Magn Reson Med. 2003; 49:216–222. [PubMed: 12541240]
72. Spielman DM, Pauly JM, Meyer CH. Magnetic resonance fluoroscopy using spirals with variable sampling densities. Magn Reson Med. 1995; 34:388–394. [PubMed: 7500878]
73. Bakker CJ, Hoogeveen RM, Weber J, van Vaals JJ, Viergever MA, Mali WP. Visualization of dedicated catheters using fast scanning techniques with potential for MR-guided vascular interventions. Magn Reson Med. 1996; 36:816–820. [PubMed: 8946346]
74. Busch M, Bornstedt A, Wendt M, Duerk JL, Lewin JS, Gronemeyer D. Fast “real time” imaging with different k-space update strategies for interventional procedures. J Magn Reson Imaging. 1998; 8:944–954. [PubMed: 9702897]
75. Shankaranarayanan A, Wendt M, Aschoff AJ, Lewin JS, Duerk JL. Radial keyhole sequences for low field projection reconstruction interventional MRI. J Magn Reson Imaging. 2001; 13:142–151. [PubMed: 11169817]
76. Pruessmann KP, Weiger M, Scheidegger MB, Boesiger P. SENSE: sensitivity encoding for fast MRI. Magn Reson Med. 1999; 42:952–962. [PubMed: 10542355]
77. Sodickson DK, Manning WJ. Simultaneous acquisition of spatial harmonics (SMASH): fast imaging with radiofrequency coil arrays. Magn Reson Med. 1997; 38:591–603. [PubMed: 9324327]
78. Elgort DR, Duerk JL. A review of technical advances in interventional magnetic resonance imaging. Acad Radiol. 2005; 12:1089–1099. [PubMed: 16099690]
79. Hundley WG, Hamilton CA, Thomas MS, et al. Utility of fast cine magnetic resonance imaging and display for the detection of myocardial ischemia in patients not well suited for second harmonic stress echocardiography. Circulation. 1999; 100:1697–1702. [PubMed: 10525488]
80. Aletras AH, Ding S, Balaban RS, Wen H. DENSE: displacement encoding with stimulated echoes in cardiac functional MRI. J Magn Reson. 1999; 137:247–252. [PubMed: 10053155]
81. Axel L, Dougherty L. Heart wall motion: improved method of spatial modulation of magnetization for MR imaging. Radiology. 1989; 172:349–350. [PubMed: 2748813]
82. Zerhouni EA, Parish DM, Rogers WJ, Yang A, Shapiro EP. Human heart: tagging with MR imaging-a method for noninvasive assessment of myocardial motion. Radiology. 1988; 169:59–63. [PubMed: 3420283]
83. Gilson WD, Yang Z, French BA, Epstein FH. Complementary displacement-encoded MRI for contrast-enhanced infarct detection and quantification of myocardial function in mice. Magn Reson Med. 2004; 51:744–752. [PubMed: 15065247]
84. Al-Saadi N, Nagel E, Gross M, et al. Noninvasive detection of myocardial ischemia from perfusion reserve based on cardiovascular magnetic resonance. Circulation. 2000; 101:1379–1383. [PubMed: 10736280]

85. Lima JA, Judd RM, Bazille A, Schulman SP, Atalar E, Zerhouni EA. Regional heterogeneity of human myocardial infarcts demonstrated by contrast-enhanced MRI. Potential mechanisms. Circulation. 1995; 92:117–1125.

86. Modo M, Mellodew K, Cash D, et al. Mapping transplanted stem cell migration after a stroke: a serial, in vivo magnetic resonance imaging study. Neuroimage. 2004; 21:311–317. [PubMed: 14741669]

87. Arbab AS, Pandit SD, Anderson SA, et al. MRI and confocal microscopy studies of magnetically labeled endothelial progenitor cells trafficking to sites of tumor angiogenesis. Stem Cells. 2006; 24:671–678. [PubMed: 16179427]

88. Soto AV, Gilson WD, Kedziorek D, et al. MRI tracking of regional persistence of feridex-labeled mesenchymal stem cells in a canine myocardial infarction model. J Cardiovasc Magn Reson. 2006; 8:89–90.

89. Stuckey DJ, Carr CA, Martin-Rendon E, et al. Iron particles for noninvasive monitoring of bone marrow stromal cell engraftment into, and isolation of viable engrafted donor cells from, the heart. Stem Cells. 2006; 24:1968–1975. [PubMed: 16627684]

90. Amado LC, Salrais AP, Schuleri KH, et al. Cardiac repair with intramyocardial injection of allogeneic mesenchymal stem cells after myocardial infarction. Proc Natl Acad Sci U S A. 2005; 102:11474–11479. [PubMed: 16061805]

91. Daldrup-Link HE, Rudelius M, Oostendorp RA, et al. Comparison of iron oxide labeling properties of hematopoietic progenitor cells from umbilical cord blood and from peripheral blood for subsequent in vivo tracking in a xenotransplant mouse model XXX. Acad Radiol. 2005; 12:502–510. [PubMed: 15831425]

92. Anderson SA, Glod J, Arbab AS, et al. Noninvasive MR imaging of magnetically labeled stem cells to directly identify neovasculature in a glioma model. Blood. 2005; 105:420–425. [PubMed: 15331444]

93. Guttman MA, Lederman RJ, Sorger JM, McVeigh ER. Real-time volume rendered MRI for interventional guidance. J Cardiovasc Magn Reson. 2002; 4:431–442. [PubMed: 12549231]

94. Wacker FK, Hillenbrand CM, Duerk JL, Lewin JS. MR-guided endovascular interventions: device visualization, tracking, navigation, clinical applications, and safety aspects. Magn Reson Imaging Clin N Am. 2005; 13:431–439. [PubMed: 16084411]

95. Bock M, Volz S, Zuhlsdorff S, et al. MR-guided intravascular procedures: real-time parameter control and automated slice positioning with active tracking coils. J Magn Reson Imaging. 2004; 19:580–589. [PubMed: 15112307]

96. Lorenz, CH.; Kirchberg, KJ.; Zuehlsdorff, S., et al. Proc ISMRM. Miami, FL: 2005. Interactive Frontend (IFE): a platform for graphical MR scanner control and scan automation; p. 2170

97. Zuehlsdorff, S.; Speier, S.; Greed, JD.; Omary, RA.; Simonetti, OP.; Li, D. Proc ISMRM. Miami, FL: 2005. An interactive real time sequence for interventional MRI; p. 2157

98. Zhang Q, Wendt M, Aschoff AJ, Zheng L, Lewin JS, Duerk JL. Active MR guidance of interventional devices with target-navigation. Magn Reson Med. 2000; 44:56–65. [PubMed: 10893522]

99. Wacker FK, Elgort D, Hillenbrand CM, Duerk JL, Lewin JS. The catheter-driven MRI scanner: a new approach to intravascular catheter tracking and imaging-parameter adjustment for interventional MRI. AJR Am J Roentgenol. 2004; 183:391–395. [PubMed: 15269031]

100. Elgort DR, Wong EY, Hillenbrand CM, Wacker FK, Lewin JS, Duerk JL. Real-time catheter tracking and adaptive imaging. J Magn Reson Imaging. 2003; 18:621–626. [PubMed: 14579407]

101. Bock M, Volz S, Zuehlsdorff S, et al. MR-guided intravascular procedures: real-time parameter control and automated slice positioning with active tracking coils. J Magn Reson Imaging. 2004; 19:580–589. [PubMed: 15112307]

102. Patel KC, Duerk JL, Zhang Q, et al. Methods for providing probe position and temperature information on MR images during interventional procedures. IEEE Trans Med Imaging. 1998; 17:794–802. [PubMed: 9874304]

103. Chung YC, Duerk JL, Shankaranarayanan A, Hampke M, Merkle EM, Lewin JS. Temperature measurement using echo-shifted FLASH at low field for interventional MRI. J Magn Reson Imaging. 1999; 9:138–145. [PubMed: 10030661]

104. Hempel E, Fischer H, Gumb L, et al. An MRI-compatible surgical robot for precise radiological interventions. Comput Aided Surg. 2003; 8:180–191. [PubMed: 15360099]

105. Krombach GA, Baireuther R, Higgins CB, Saeed M. Distribution of intramyocardially injected extracellular MR contrast medium: effects of concentration and volume. Eur Radiol. 2004; 14:334–340. [PubMed: 14618368]

106. Saeed M, Saloner D, Weber O, Martin A, Henk C, Higgins C. MRI in guiding and assessing intramyocardial therapy. Eur Radiol. 2005; 15:851–863. [PubMed: 15856250]

107. Strauer BE, Brehm M, Zeus T, et al. Repair of infarcted myocardium by autologous intracoronary mononuclear bone marrow cell transplantation in humans. Circulation. 2002; 106:1913–1918. [PubMed: 12370212]

108. Assmus B, Schachinger V, Teupe C, et al. Transplantation of progenitor cells and regeneration enhancement in acute myocardial infarction (TOPCARE-AMI). Circulation. 2002; 106:3009–3017. [PubMed: 12473544]

109. Britten MB, Abolmaali ND, Assmus B, et al. Infarct remodeling after intracoronary progenitor cell treatment in patients with acute myocardial infarction (TOPCARE-AMI): mechanistic insights from serial contrast-enhanced magnetic resonance imaging. Circulation. 2003; 108:2212–2218. [PubMed: 14557356]

110. Wollert KC, Meyer GP, Lotz J, et al. Intracoronary autologous bone-marrow cell transfer after myocardial infarction: the BOOST randomised controlled clinical trial. Lancet. 2004; 364:141–148. [PubMed: 15246726]

111. Bartunek J, Vanderheyden M, Vandekerckhove B, et al. Intra-coronary injection of CD133-positive enriched bone marrow progenitor cells promotes cardiac recovery after recent myocardial infarction: feasibility and safety. Circulation. 2005; 112(9 Suppl):I178–I183. [PubMed: 16159812]

112. Lunde K, Solheim S, Aakhus S, Arnesen H, Abdelnoor M, Forfang K. Autologous stem cell transplantation in acute myocardial infarction: the ASTAMI randomized controlled trial. Intracoronary transplantation of autologous mononuclear bone marrow cells, study design and safety aspects. Scand Cardiovasc J. 2005; 39:150–158. [PubMed: 16152682]

113. Schachinger V, Erbs S, Elsasser A, et al. Intracoronary bone marrow-derived progenitor cells in acute myocardial infarction. N Engl J Med. 2006; 355:1210–1221. [PubMed: 16990384]

114. Janssens S, Dubois C, Bogaert J, et al. Autologous bone marrow-derived stem-cell transfer in patients with ST-segment elevation myocardial infarction: double-blind, randomised controlled trial. Lancet. 2006; 367:113–121. [PubMed: 16413875]

115. Lunde K, Solheim S, Aakhus S, et al. Intracoronary injection of mononuclear bone marrow cells in acute myocardial infarction. N Engl J Med. 2006; 355:1199–1209. [PubMed: 16990383]

116. Meyer GP, Wollert KC, Lotz J, et al. Intracoronary bone marrow cell transfer after myocardial infarction: eighteen months' follow-up data from the randomized, controlled BOOST (bone marrow transfer to enhance ST-elevation infarct regeneration) trial. Circulation. 2006; 113:1287–1294. [PubMed: 16520413]

117. Assmus B, Honold J, Schachinger V, et al. Transcoronary transplantation of progenitor cells after myocardial infarction. N Engl J Med. 2006; 355:1222–1232. [PubMed: 16990385]

118. Goussetis E, Manginas A, Koutelou M, et al. Intracoronary infusion of CD133+ and CD133-CD34+ selected autologous bone marrow progenitor cells in patients with chronic ischemic cardiomyopathy: cell isolation, adherence to the infarcted area, and body distribution. Stem Cells. 2006; 24:2279–2283. [PubMed: 16794269]

119. Katritsis DG, Sotiropoulou PA, Karvouni E, et al. Transcoronary transplantation of autologous mesenchymal stem cells and endothelial progenitors into infarcted human myocardium. Catheter Cardiovasc Interv. 2005; 65:321–329. [PubMed: 15954106]

120. Hou D, Youssef EA, Brinton TJ, et al. Radiolabeled cell distribution after intramyocardial, intracoronary, and interstitial retrograde coronary venous delivery: implications for current clinical trials. Circulation. 2005; 112(9 Suppl):I150–I156. [PubMed: 16159808]

121. Fuchs S, Satler LF, Kornowski R, et al. Catheter-based autologous bone marrow myocardial injection in no-option patients with advanced coronary artery disease: a feasibility study. J Am Coll Cardiol. 2003; 41:1721–1724. [PubMed: 12767654]

122. Perin EC, Dohmann HF, Borojevic R, et al. Transendocardial, autologous bone marrow cell transplantation for severe, chronic ischemic heart failure. Circulation. 2003; 107:2294–2302. [PubMed: 12707230]

123. Tse HF, Kwong YL, Chan JK, Lo G, Ho CL, Lau CP. Angiogenesis in ischaemic myocardium by intramyocardial autologous bone marrow mononuclear cell implantation. Lancet. 2003; 361:47–49. [PubMed: 12517468]

124. Perin EC, Dohmann HF, Borojevic R, et al. Improved exercise capacity and ischemia 6 and 12 months after transendocardial injection of autologous bone marrow mononuclear cells for ischemic cardiomyopathy. Circulation. 2004; 110(11 Suppl 1):II213–II218. [PubMed: 15364865]

125. Lima J, Judd R, Schulman D, Atalar E, Lugo-Oliveri C, Zerhouni E. Capillary damage with human infarcts assessed by contrast-enhanced MRI indexes greater myocardial dysfunction and greater myocardial loss. Circulation. 1994; 904:I410.

126. Kim RJ, Chen EL, Lima JA, Judd RM. Myocardial Gd-DTPA kinetics determine MRI contrast enhancement and reflect the extent and severity of myocardial injury after acute reperfused infarction. Circulation. 1996; 94:3318–3326. [PubMed: 8989146]

127. Barbash IM, Leor J, Feinberg MS, et al. Interventional magnetic resonance imaging for guiding gene and cell transfer in the heart. Heart. 2004; 90:87–91. [PubMed: 14676253]

128. Rickers C, Kraitchman D, Fischer G, Kramer HH, Wilke N, Jerosch-Herold M. Cardiovascular interventional MR imaging: a new road for therapy and repair in the heart. Magn Reson Imaging Clin N Am. 2005; 13:465–479. [PubMed: 16084413]

129. Gilson WD, Bulte JWM, Hofmann LV, et al. Magnetic resonance fluorscopy for precise targeting and monitoring of mesenchymal stem cell engraftment combined with serial MRI to assess efficacy. Am J Cardiol. 2005; 96:72H.

130. Bellenger NG, Davies LC, Francis JM, Coats AJ, Pennell DJ. Reduction in sample size for studies of remodeling in heart failure by the use of cardiovascular magnetic resonance. J Cardiovasc Magn Reson. 2000; 2:271–278. [PubMed: 11545126]

131. Jugdutt BI, Amy RW. Healing after myocardial infarction in the dog: changes in infarct hydroxyproline and topography. J Am Coll Cardiol. 1986; 7:91–102. [PubMed: 3941223]

132. Moelker AD, Baks T, van den Bos EJ, et al. Reduction in infarct size, but no functional improvement after bone marrow cell administration in a porcine model of reperfused myocardial infarction. Eur Heart J. 2006; 27:3057–3064. [PubMed: 17135284]

133. Limbourg FP, Ringes-Lichtenberg S, Schaefer A, et al. Haematopoietic stem cells improve cardiac function after infarction without permanent cardiac engraftment. Eur J Heart Fail. 2005; 7:722–729. [PubMed: 16158493]

134. Zeng L, Hu Q, Wang X, et al. Bioenergetic and functional consequences of bone marrow-derived multipotent progenitor cell transplantation in hearts with postinfarction left ventricular remodeling. Circulation. 2007; 115:1866–1875. [PubMed: 17389266]

135. Jiang Y, Jahagirdar BN, Reinhardt RL, et al. Pluripotency of mesenchymal stem cells derived from adult marrow. Nature. 2002; 418:41–49. [PubMed: 12077603]

136. Holden C. Stem cells. Data on adult stem cells questioned. Science. 2007; 315:1207. [PubMed: 17332385]

137. Gilson WD, Soto AV, Kedziorek D, et al. Mesenchymal stem cell therapy in a canine myocardial infarction model: assessment of regional persistence and function using MRI. Circ Res. 2006; 99:E50.

138. Smits PC, van Geuns RJ, Poldermans D, et al. Catheter-based intramyocardial injection of autologous skeletal myoblasts as a primary treatment of ischemic heart failure: clinical experience with six-month follow-up. J Am Coll Cardiol. 2003; 42:2063–2069. [PubMed: 14680727]

139. Schachinger V, Assmus B, Britten MB, et al. Transplantation of progenitor cells and regeneration enhancement in acute myocardial infarction: final one-year results of the TOPCARE-AMI Trial. J Am Coll Cardiol. 2004; 44:1690–1699. [PubMed: 15489105]

140. Hendrikx M, Hensen K, Clijsters C, et al. Recovery of regional but not global contractile function by the direct intramyocardial autologous bone marrow transplantation: results from a randomized controlled clinical trial. Circulation. 2006; 114(1 Suppl):I101–I107. [PubMed: 16820557]

141. van den Bos EJ, Baks T, Moelker AD, et al. Magnetic resonance imaging of haemorrhage within reperfused myocardial infarcts: possible interference with iron oxide-labelled cell tracking? Eur Heart J. 2006; 27:1620–1626. [PubMed: 16751204]

142. Kustermann E, Roell W, Breitbach M, et al. Stem cell implantation in ischemic mouse heart: a high-resolution magnetic resonance imaging investigation. NMR Biomed. 2005; 18:362–370. [PubMed: 15948224]

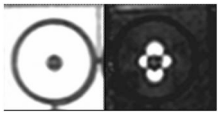

Figure 1.
Fast spin echo image of one million iron oxide-labeled mesenchymal stem cells, which appear hypointense in an agarose phantom (left). Using a positive contrast imaging technique (25) the iron oxide-labeled stem cells appear hyperintense in a typical dipole pattern (right).

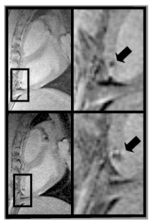

Figure 2.
Long-axis MR images (left) of the left ventricle with magnified view (right) showing hypointense lesions (arrow) caused by iron oxide-labeled mesenchymal stem cells injected under x-ray fluoroscopy acquired within 24 hours (top) and 1 week (bottom) of injection. Expansion of the hypointense region at 1 week is indicative of local migration of the stem cells. Adapted from Kraitchman et al (38), which contains expanded contiguous image data and histological validation.

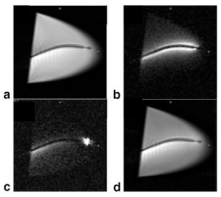

Figure 3.
Long-axis MR images (4.0 msec repetition time, 2.0 msec echo time, 70° flip angle, 240 mm^2 field of view, 160 × 160 matrix, 8 mm section thickness, 2 frames per second) acquired in water bath containing nitinol catheter and different active coil elements. **a:** Only the external surface coil elements were active. **b:** Only the catheter coil was active. **c:** Only the catheter tip microcoil was active. **d:** Both surface coil elements and active catheter coil are contributing to the image. Reprinted with permission from Saeed et al (65).

Figure 4.
Screen capture of the Siemens prototype Interactive Front End (IFE) graphical interface that enables real-time scan plane manipulation and serial acquisition of up to three imaging planes. The image is reconstructed with the active injection catheter colored green for enhanced visibility. Representative pseudo long- and short-axis images are shown acquired in real-time in vivo in a canine reperfused myocardial infarction. Bookmark images (small images at bottom) facilitate rapid return to previous scan plane position using a simple drag-n-drop of the image plane into one of three image acquisition planes.

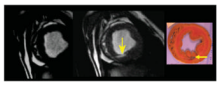

Figure 5.
High-resolution, ECG-gated, breath-hold steady-state free precession short-axis images prior to contrast injection (left), and after transmyocardial gadolinium-based contrast injection with tissue vital dye (middle) under MR fluoroscopy. Postmortem digital image (right) demonstrates a high concordance of the spatial location and extent with in vivo MRI.

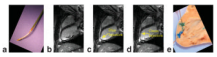

Figure 6.
a: The distal tip of a custom, MR-compatible active injection catheter (66) that was used for injections of 10% gadolinium with a tissue vital dye. **b:** ECG-gated, breath-hold long-axis image prior to injection. **c:** Long-axis image after first gadolinium injection mixed with a blue dye. **d:** Long-axis image after second gadolinium injection with green dye. Unfortunately, injection sites can only be appreciated for a short period of time due to wash-out of the gadolinium contrast agent. **e:** Postmortem image demonstrating distinct injection sites. Adapted from Karmarkar et al (66).

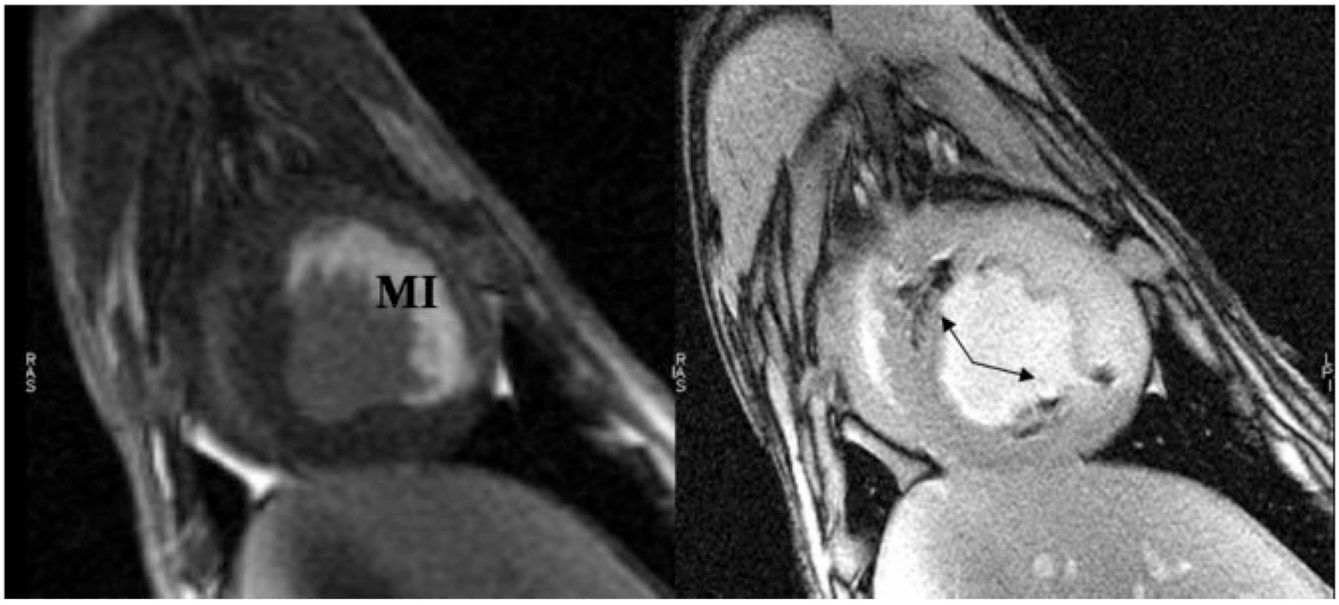

Figure 7.
Targeting of the iron oxide-labeled stem cell injections to the peri-infarction area was performed based on delayed contrast-enhanced short-axis MRI (left) in which hyperintense signal represents myocardial infarction (MI) in this acute, reperfused canine model. Short-axis, high-resolution fast gradient echo image (right) of the left ventricle demonstrating multiple hypointensities (arrows) from iron oxide-labeled mesenchymal stem cells that were injected under MR fluoroscopy. Adapted from Bulte and Kraitchman (17).

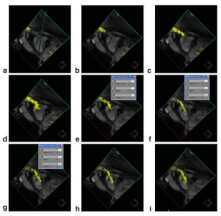

Figure 8.
Still-frame captures of three-plane view from the Siemens interactive graphical interface demonstrating guiding an active catheter into the left ventricle from a carotid artery approach. Images were acquired with a nongated steady-state free precession pulse sequence. The needle of the injection catheter is colored yellow. In frame (**f**) the gain from the active catheter is reduced to enable better determination of the catheter position.

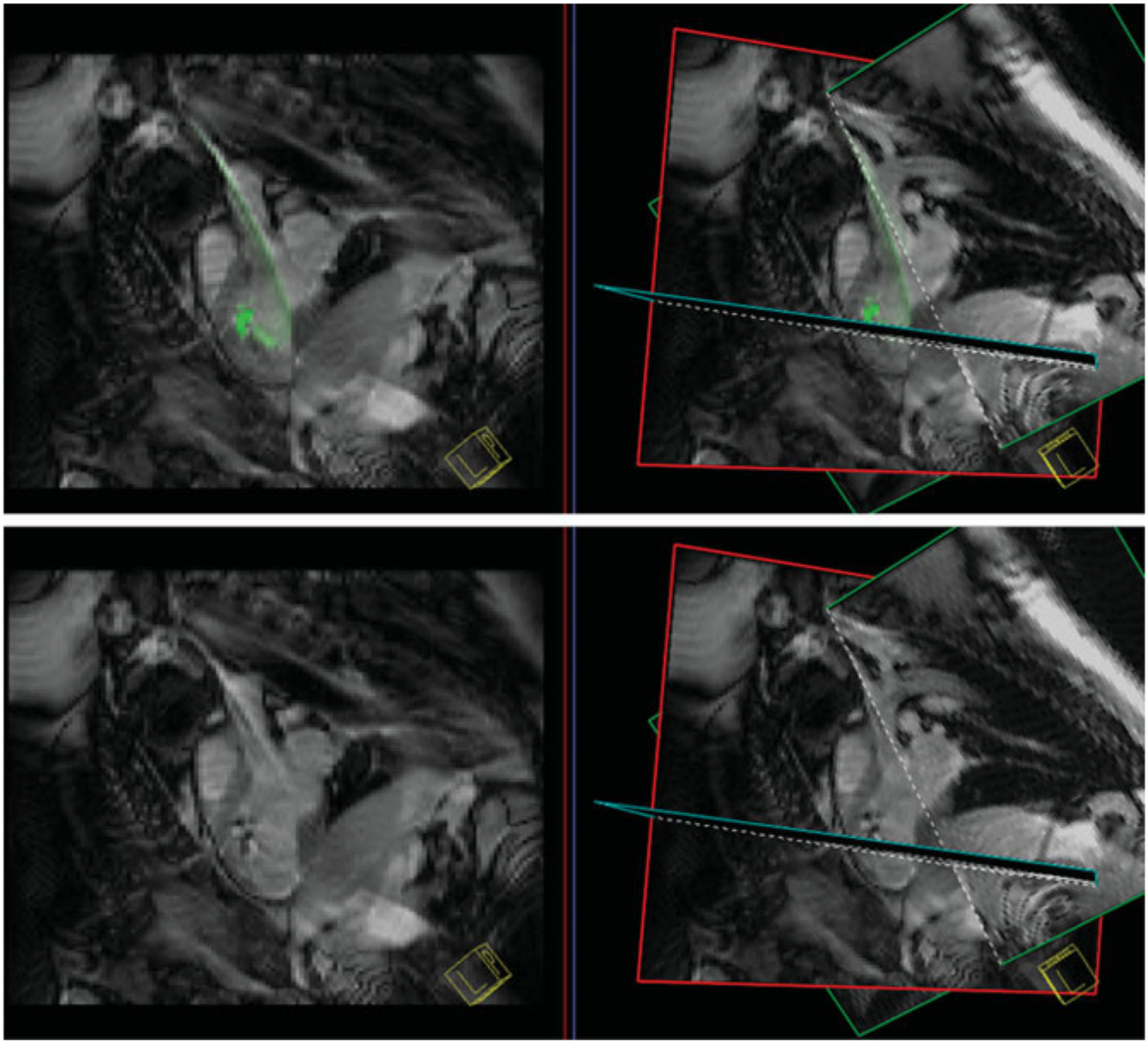

Figure 9.

Top: A single pseudo-long axis-plane (left) and three-plane view (right) with an injection catheter shown in green prior to labeled stem cell injection. The catheter is steerable and flexible to enable access to many portions of the left ventricular endocardial surface. Bottom: During injection of iron oxide-labeled stem cells the active catheter gain is no longer colored to enhance detection of hypointensities in the myocardium to document stem cell injection success.

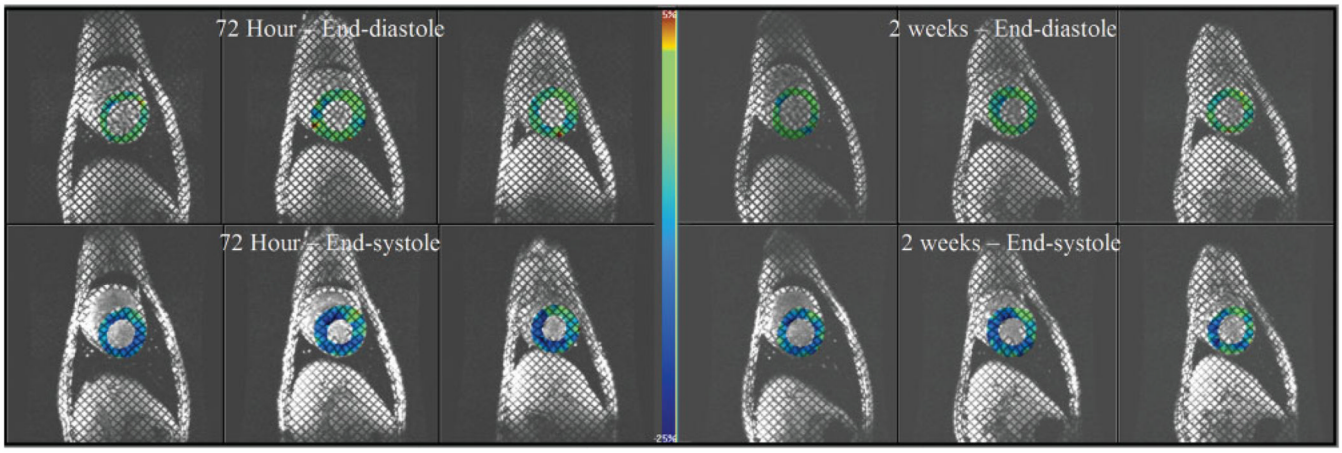

Figure 10.
Three representative short-axis images at end-diastole (top row) and end-systole (bottom row) in a dog with a reperfused left anterior descending coronary artery myocardial infarction that received transmyocardially administered mesenchymal stem cells under MR fluoroscopy. Prior to injection at 72 hours postinfarction (images on left), tagged MRI with circumferential strain shown as a color overlay where less shortening is green and more shortening is blue demonstrates a mild functional defect in the anteroseptal wall (12 o'clock to 2 o'clock) that shows little functional improvement or slight worsening of function at 2 weeks posttransmyocardial mesenchymal stem cell delivery (images on right).